

# Photoconductivity of Bulk-Film-Based Graphene Sheets

Xin Lv, Yi Huang, Zhibo Liu, Jianguo Tian, Yan Wang, Yanfeng Ma, Jiajie Liang, Shipeng Fu, Xiangjian Wan, and Yongsheng Chen\*

*Time-resolved photoconductivity measurements are carried out on graphene films prepared by using soluble graphene oxide. High photocurrent generation efficiency is observed for these graphene-based films, and the relationships between their photoconductivity and different preparation methods, incident light intensity, external electric field, and photon energies are investigated. Higher photoconductivity is observed with higher photon energy at same incident light intensity. By fitting the experimental data to the Onsager model, the primary quantum yields for charge separation to generate bound electron–hole pairs and the initial ion-pair thermalization separation distance are calculated.*

## Keywords:

- carbon nanotubes
- drop-cast films
- graphene
- photoconductivity
- spin-coated films

## 1. Introduction

Graphene, a single layer of  $sp^2$ -bonded carbon atoms packed into a benzene-ring structure, is a nearly ideal 2D material.<sup>[1,2]</sup> Recent research indicates that graphene sheets offer extraordinary electronic,<sup>[3–5]</sup> thermal,<sup>[6]</sup> and mechanical<sup>[7,8]</sup> properties and are expected to provide a variety of applications in various technological fields,<sup>[9]</sup> such as field-effect transistors,<sup>[10,11]</sup> transparent conductors,<sup>[12,13]</sup> electro-mechanical resonators,<sup>[14]</sup> and drug delivery.<sup>[15]</sup> It is reported that the room-temperature mobility of graphene reaches over  $10\,000\text{ cm}^2\text{ V}^{-1}\text{ s}^{-1}$ , and that single-layer graphene is in theory a zero-gap semiconductor that offers ballistic transport at submicrometer distances.<sup>[16]</sup> As expected, its optoelectronic properties are of particular interest and importance in academic as well as technological and industrial sectors. Recently, we have reported its photovoltaic and nonlinear optical limiting applications using soluble graphene materi-

als.<sup>[17,18]</sup> Theoretically, the photoconductivity of graphene should be fairly strong because the intrinsic character of graphene exhibits a maximum of the dark resistance,<sup>[19]</sup> and Mak et al. have already measured the optical conductivity of single-crystal graphene on a  $\text{SiO}_2$  substrate.<sup>[20]</sup> Studies on bulk films of graphene are expected to provide opportunities for constructing various devices with practical applications. With a similar structure to graphene, bulk single-walled carbon nanotube (SWNT) films have been reported to show good photoconductivity,<sup>[21–23]</sup> but the coexistence of semiconducting and metallic SWNTs and the existence of inherited impurities have been hindering their photoconductivity performance and applications.<sup>[24]</sup> In this paper we report the photoconductivity of bulk films of graphene sheets upon laser illumination. Our results clearly show that microscale thin films of graphene can act as a semiconductor with strong photoconductivity.

## 2. Results and Discussion

The starting material graphene oxide (GO) is synthesized by oxidation of graphite with a modified Hummers method.<sup>[12,17,25]</sup> Heavy oxygenation of graphite in this process results in multifunctional groups on the basal planes and at the sheet edges, which makes GO sheets strongly hydrophilic and easily dispersible at the state of complete exfoliation with almost entire single-layered graphene sheets in water.<sup>[26]</sup> The thickness of these graphene sheets has been investigated by a large number of atomic force microscopy (AFM) studies and found to be in the range of 0.8 to 1.0 nm (Figure 1A), which is the typical thickness for the individual

[\*] Prof. Y.-S. Chen, X. Lv, Prof. Y. Huang, Y. Wang, Prof. Y.-F. Ma, J.-J. Liang, Dr. X.-J. Wan  
Key Laboratory of Functional Polymer Materials and Center for Nanoscale Science and Technology  
Institute of Polymer Chemistry, College of Chemistry  
Nankai University Tianjin, 300071 (China)  
E-mail: yschen99@nankai.edu.cn  
Dr. Z.-B. Liu, Prof. J.-G. Tian, S.-P. Fu  
Key Laboratory of Weak Light Nonlinear Photonics  
Ministry of Education  
Teda Applied Physics School, Nankai University  
Tianjin 300071 (China)

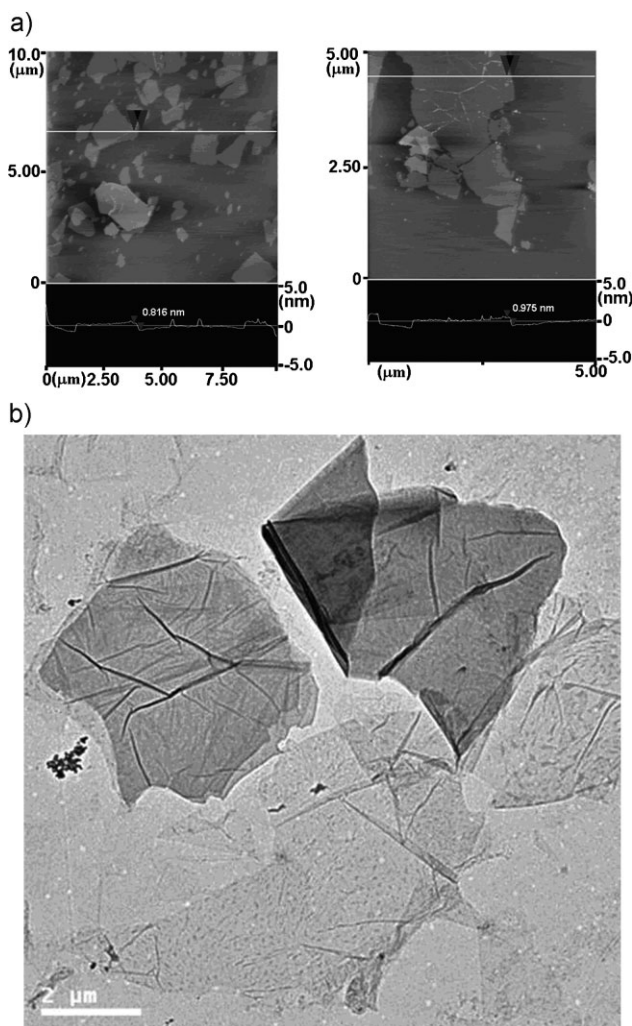


**Figure 1.** A) Tapping mode AFM images and height profiles of deposited GO films. B) TEM image of GO.

and functionalized graphene sheets.<sup>[11,12]</sup> The length and width dimensions are mostly in the range of thousands of nanometers. These results are also supported by transmission electron microscopy (TEM) analysis (Figure 1B). For further device applications, it has been demonstrated that the aromatic conjugation structure of graphene can be largely restored and its electrical conductivity can be significantly increased by chemical reduction and/or annealing of GO.<sup>[12,27]</sup> A certain amount of defects would still exist on these graphene sheets after the chemical reduction or/and annealing.

To illuminate the variation of graphene structure after the chemical reduction and annealing process, we examined Raman and UV–Vis–NIR spectra of graphene films before and after reduction. As shown in Figure 2, the structural change during the chemical process of oxidation and reduction of exfoliated graphene sheets is reflected in the Raman spectra. For graphite, the main peak at  $1581\text{ cm}^{-1}$  (G-band) can be observed, which is assigned to the first-order scattering of the  $E_{2g}$  mode. A slight frequency shift ( $\approx 9\text{ cm}^{-1}$ ) toward a higher wavenumber and a broadened bandwidth of the G-band are found in GO and reduced GO compared with

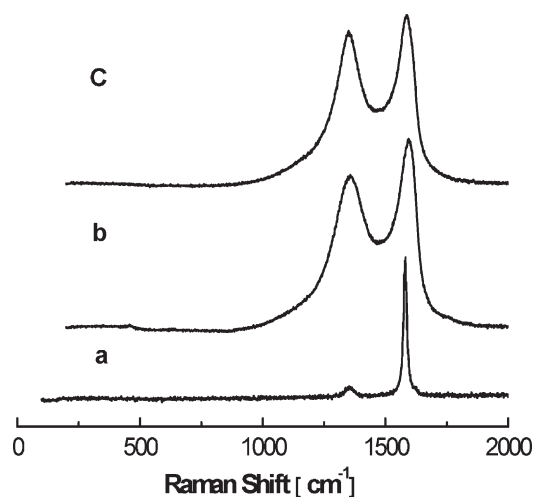


**Figure 2.** The Raman spectra of a) graphite, b) GO, and c) reduced and annealed GO.

graphite, indicating the decrease of in-plane graphene size during the chemical reaction process.<sup>[28]</sup> There is no obvious frequency shift of the G-band ( $\approx 1590\text{ cm}^{-1}$ ) and D-band ( $\approx 1355\text{ cm}^{-1}$ ) before and after the reduction, but the D/G intensity ratio of the reduced GO is increased compared to GO, which is in accordance with previous reports.<sup>[29]</sup>

Figure 3 shows the UV–Vis–NIR spectra of the GO solution, GO film, and graphene sheet film. The bathochromic shift (77 nm) of the absorption maximum of the GO film ( $\lambda_{\text{max}} = 302\text{ nm}$ ) compared to that of the GO solution ( $\lambda_{\text{max}} = 225\text{ nm}$ ) suggests an extended  $\pi$ -stacking interlayer conjugation arising from solution to film for the exfoliated GO. While a featureless absorption spectrum is observed for the graphene film, the absorption in the whole spectral region increases significantly, indicating that much of the electronic conjugation within the graphene sheets is restored.

The restoration of  $\pi$ -conjugation for graphene sheets through the reduction and annealing process gives this material a similar chemical structure to the large fused polyaromatic “graphene molecules” reported by Mullen

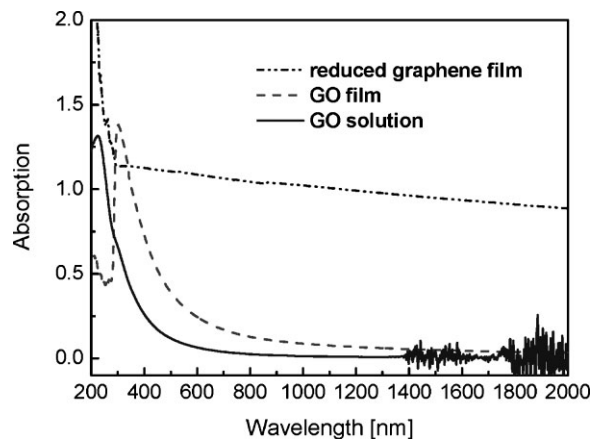


**Figure 3.** UV–Vis–NIR absorption spectra of GO solution ( $0.05\text{ mg mL}^{-1}$ ), GO, and graphene sheet film (drop-cast film).

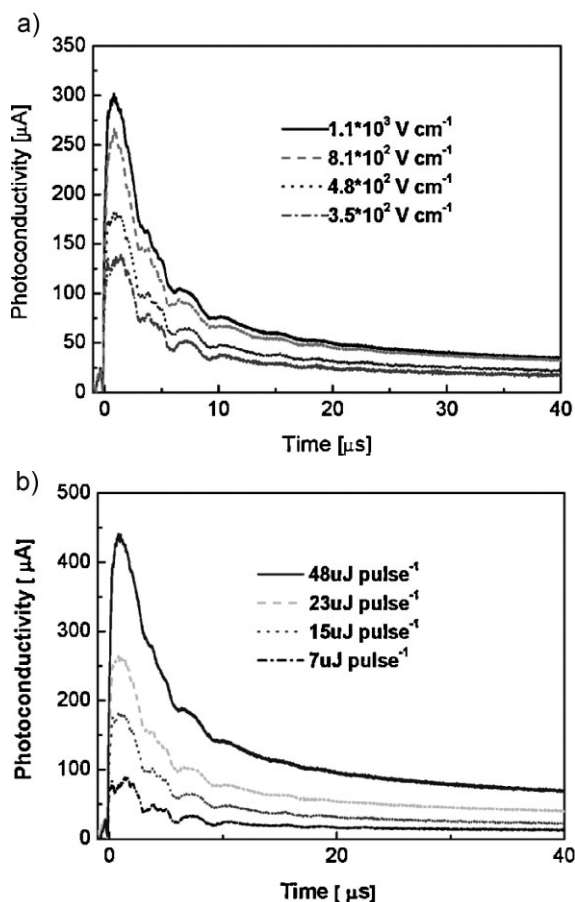


Figure 4. Transient photocurrents measured on a typical drop-cast graphene film (155-nm thickness) under a photon energy of 2.33 eV at different electric fields and an incident light intensity of  $15 \mu\text{J}$  per pulse (A), and at different light intensities at an electric field of  $4.8 \times 10^2 \text{ V cm}^{-1}$  (B).

et al.<sup>[30]</sup> and other groups. The reduction and annealing should remove most of the organic functional groups as reported earlier.<sup>[29]</sup> It has been reported that these semiconductor materials, with 2D graphene molecular structures, exhibit many interesting and excellent optoelectronic properties. Figure 4 shows the typical transient photoconductivity results of drop-casting graphene films with various intensities of incident light and external electric field under photon energy of 2.33 eV. The films are prepared from GO water solution by drop-casting, followed by reduction and annealing as detailed later. A strong photoconductivity response of less than  $10 \mu\text{s}$  can be observed and its peak height increases with the increase of incident light intensity or external electric field, indicating that the charge carrier generation is influenced by the number of photons and the external field intensity. The decay time of the photocurrent shows changes somewhat depending on variation of excitation intensity and applied electric field. This could be because more time is needed to recombine more charge carriers generated by the increased external field and light intensity.

The Onsager model has been used widely to analyze the features of photogenerated charge carriers.<sup>[31]</sup> Under a modified kinetic model<sup>[32]</sup> with the field-assisted dissociation

of photoexcited states, the photoexcited state can disappear by dissociation into free carriers with an electrical-field ( $E$ )-dependent rate constant  $k_d(E)$  or by decay to the ground state with rate constant  $k_f$ . The photocurrent generation efficiency  $P(E)$  of a photoconductor can be given by Equation (1)

$$P(E) = k_d(E) / [k_f + k_d(E)] \quad (1)$$

The model assumes that the absorption of a photon creates a bound geminate charge pair with a thermalization separation distance of  $r_0$ , and the fraction of absorbed photons for generating bound electron-hole pairs is the primary quantum yield  $\phi_0$ , which is assumed to be field-independent. By fitting the experimental data to the Onsager model, we obtained values of  $r_0 = 1.4 \text{ nm}$  and  $\phi_0 = 0.9$ . These values are comparable with that of the photoconductivity for the film of fullerene ( $\text{C}_{60}$ ) composite with poly(vinylcarbazole) (PVK), where the thermalization length and primary quantum yield are 1.9 nm and 0.9, respectively.<sup>[33]</sup>

Figure 5 shows the relationships between photocurrent peak height with incident light intensity and external electric fields for various photon energies. As shown in Figure 5A, the photoconductivity peak height responds linearly to incident light intensity during the range we measured at the same electrical field for all different photon energies. Comparing the

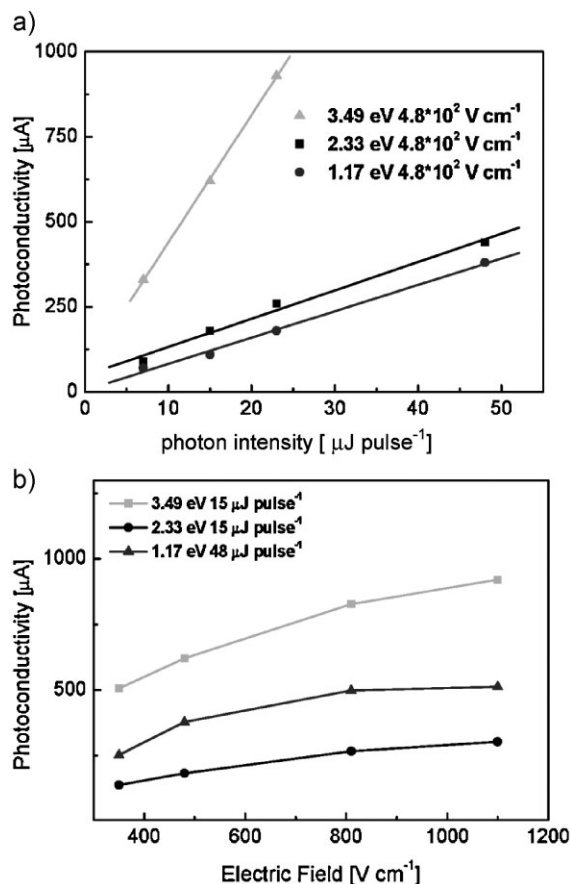
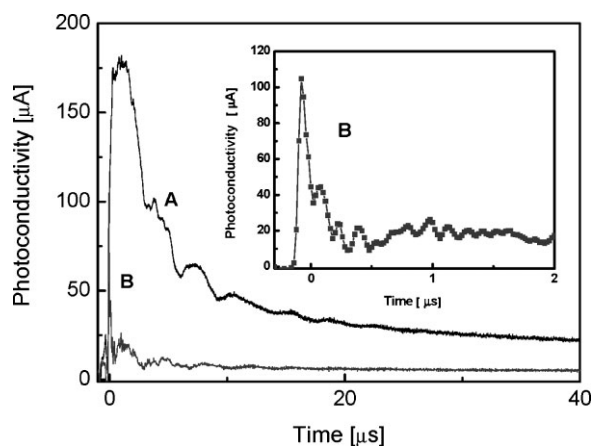


Figure 5. A) Incident light intensity and B) external electric field dependence of photoresponse with different photon energies for the drop-cast graphene film.

photoconductivity for different photon energies at the same light intensity, it can be concluded that the graphene film generates more charge carriers per unit volume when it is irradiated with higher photon energy, which is in accordance with the results reported by Mak et al.<sup>[20]</sup> This indicates that graphene may have a strong photoconductivity response for all the wavelengths in the measured range, corresponding to the strong absorption in the wide frequency range. This is quite different from the photoconductivity of SWNTs<sup>[23,34]</sup> and C<sub>60</sub>,<sup>[33,35]</sup> where the strong wavelength dependence and clear peaks corresponding to their absorption spectra are observed. It is well-known that the band structure of SWNTs depends on their chirality and diameter. From a chemical point of view, the graphene sheets prepared in this work should be a mixture of many large fused aromatic molecules, which have very similar structure but with some minor differences of size, shape, and edge groups. Thus, these graphene molecules should have similar but slightly different absorption spectra in a certain scope. The observed photoconductivity of graphene films is the overall response of all these slightly different graphene sheets. Also we should note that perfect graphene has a symmetrical valence and conduction band structure joined at the Dirac point, which is described by a Dirac spectrum.<sup>[1]</sup> Thus, we believe that both the intrinsic band structure features of graphene and the existence of various slightly different graphene sheets mentioned above may play an important role in the dependence of photoconductivity on photon energy.

Though more photocurrent is generated with higher photon energy under the same electrical field, the photoconductivity intensity does not show linear dependence on the external electric field as observed in Figure 5B. It increases with the enhanced electric field to the trend of saturation, suggesting that graphene lacks replenishment of carriers to a certain extent.<sup>[23]</sup>

The peak height and decay time of the transient photoconductivity also depend on the method of film fabrication. In Figure 6, the transient waveforms for spin-coated and drop-cast films of graphene are compared. As can



**Figure 6.** Transient photocurrents measured on A) drop-cast and B) spin-coated graphene under a photon energy of 2.33 eV. The incident photon dose is 15  $\mu\text{J}$  per pulse and the external electric field is  $4.8 \times 10^2 \text{ V cm}^{-1}$ . The inset is the magnification of (B).

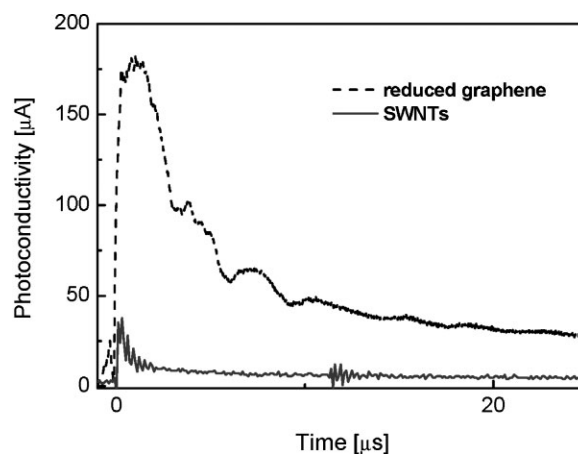


**Figure 7.** Transient photocurrents measured on drop-cast graphene and SWNT films under the same photon energy of 2.33 eV. The incident photon dose is 15  $\mu\text{J}$  per pulse and the external electric field is  $4.8 \times 10^2 \text{ V cm}^{-1}$ .

be seen, the photocurrent peak height for the drop-cast film is nearly twice of that for the spin-coated film, and the drop-cast film also has a considerably extended photoconductivity decay time. Detailed studies on film morphology, film thickness, and electrical resistance impact are needed to elucidate the reasons for these differences. However, we argue that the better morphology of the drop-cast film due to slower solvent evaporation may play an important role, since an enhanced charge carrier mobility can be expected for a better morphology as observed in many related studies.<sup>[36]</sup>

For comparison, we also measured the photoconductivity of SWNT films under the same experimental conditions of the drop-cast graphene film. As shown in Figure 7, the photoconductivity intensity of graphene is much higher than that of SWNTs under the same conditions. The graphene film also presented a much longer delay time. These results demonstrate that graphene sheets exhibit much better photoconductivity than SWNTs. Several reasons may be responsible for this result. Firstly, the existence of metallic SWNTs in the SWNT film will hinder the photocurrent generation.<sup>[37]</sup> However, both theoretical and experimental results have demonstrated that graphene acts only as a semiconductor,<sup>[11]</sup> leading to more carriers generated and less charge carriers quenched under the same illumination conditions. Secondly, the purity of the samples always has a great effect on device performance. In the mass-produced process, both catalysts and high-temperature reaction conditions limit the purity of SWNTs. Metal and amorphous carbon are hard to remove completely even by various severe chemical and physical methods, and these impurities always play a role in quenching the separated electrons and holes. For graphene, during the initial oxidation process of graphite, some heteroatoms such as oxygen are brought into the graphene structure that can be eliminated almost entirely in the following reduction and annealing steps.<sup>[12]</sup> More importantly, metal impurities will not play a role in the graphene case. Thirdly, in the case of SWNTs, the tubular structure makes the contact areas among SWNTs (bundles) small in the film.<sup>[38]</sup> However, for graphene,

the large planar 2D sheets would favor the dissociated electrons and the holes would migrate to the electrodes. Another reason, which we believe has a very important implication, is that the easy and true homogeneous dispersion of the graphene precursor GO in water makes it possible to have a more homogeneous film of graphene than of SWNTs.

### 3. Conclusions

In conclusion, excellent photoconductivity of a bulk film of graphene sheets has been observed. The results show that the photoconductivity of graphene increases with increasing light intensity and external electric field under the same photon energy. More importantly, stronger photoconductivity is also observed with higher photon energy under same light intensity and electric field. We argue that the intrinsic and unusual symmetrical cone-like band structure of graphene and the existence of various slightly different graphene sheets (size, shape, edge groups, etc.) should be part of the reason. While more detailed work is needed on the impact of film preparation and morphology, the current results demonstrate a high photocurrent generation efficiency of graphene, better than SWNTs at least in bulk films. The excellent photoconductivity of this nanoscale 2D graphene material affirms its excellent optoelectronic capability and electron transport characters. Its solution processing capability at high purity will make graphene especially suited for many applications in various optoelectronic devices.

### 4. Experimental Section

**Materials and characterization:** Graphite was obtained from Qingdao Huarun graphite Co., Ltd. with a particle size of 20  $\mu\text{m}$ . GO was prepared from graphite by the modified Hummers method.<sup>[12,17,25]</sup> SWNTs were synthesized by the arcing discharge method in our lab and purified using acid treatment.<sup>[39]</sup> Tapping mode AFM measurements were performed using a Multimode SPM from Digital Instruments with a Nanoscope IIIa Controller. The samples for AFM images were prepared by depositing a dispersion of GO/H<sub>2</sub>O solution (0.2 mg mL<sup>-1</sup>) on a freshly cleaved mica surface and allowing it to dry under ambient conditions. TEM was performed using a Philips T20ST electron microscope at an acceleration voltage of 200 kV. Raman spectra were measured by a Renishaw inVia Raman microscope at room temperature with the 514-nm line of an Ar ion laser as an excitation source. UV-Vis-NIR spectra were recorded on a JASCO V-570 spectrophotometer with the measurement range of  $\approx 200$ –2000 nm.

**Fabrication of graphene and SWNT films:** For preparing graphene films for photoconductivity measurements, the suspension of GO in water was dropped (5 mg mL<sup>-1</sup>) or spun (8 mg mL<sup>-1</sup>) on a glass substrate. After drying in vacuum for 3 h at 80 °C, the films were placed in a hydrazine vapor atmosphere for 24 h for an initial chemical reduction. Further thermal treatment was applied by annealing the reduced films in argon flow at 400 °C for 4 h to prepare the graphene film for photoconductivity and other measurements. The typical thickness of the spin-coated films

was  $\approx 10$  nm as measured using AFM in tapping mode, and that of the drop-cast films was  $\approx 155$  nm as measured with a surface profilometer (KLA-Tencor P-10). The top electrodes, typically a 100-nm-thick Au layer, were evaporated in vacuum onto the surface of the graphene films, and the gap width between Au electrodes was 30  $\mu\text{m}$ . As a comparison, SWNT films were also fabricated using the same procedure. A SWNT suspension in water (2 mg mL<sup>-1</sup>) was dropped onto a glass substrate and then the same fabrication process was applied. The thickness of the SWNT film was  $\approx 144$  nm.

**Photoconductivity measurements:** The excitation source was a pulsed Nd:YAG laser (Continuum Surelite II) with photon energies of 3.49 eV (355 nm), 2.33 eV (532 nm), and 1.17 eV (1064 nm). The pulse duration was 5 ns and the repetition frequency was 10 Hz. The bias voltages applied on the film samples in the experiment were varied from 1 to 4 V from a DC power supply. The temporal profiles of the laser pulse and the photoconductivity were monitored with 1 M ohm terminated 500 MHz digital oscilloscope (Tektronix DPO 4054). All measurements were carried out in air at room temperature, and the resistance in the dark was  $\approx 60$   $\Omega$  for the drop-cast graphene film,  $\approx 900$   $\Omega$  for the spin-coated graphene film, and  $\approx 15$   $\Omega$  for the SWNT film.

### Acknowledgements

The authors gratefully acknowledge the financial support from the NSFC (#20774047), MoST (#2006CB932702), and NSF of Tianjin City (#07JCYBJC03000, #08JCZDJC25300) of China.

- [1] A. K. Geim, K. S. Novoselov, *Nat. Mater.* **2007**, *6*, 183.
- [2] K. S. Novoselov, A. K. Geim, S. V. Morozov, D. Jiang, Y. Zhang, S. V. Dubonos, I. V. Grigorieva, A. A. Firsov, *Science* **2004**, *306*, 666.
- [3] K. S. Novoselov, Z. Jiang, Y. Zhang, S. V. Morozov, H. L. Stormer, U. Zeitler, J. C. Maan, G. S. Boebinger, P. Kim, A. K. Geim, *Science* **2007**, *315*, 1379.
- [4] D. A. Abanin, L. S. Levitov, *Science* **2007**, *317*, 641.
- [5] Y. B. Zhang, Y. W. Tan, H. L. Stormer, P. Kim, *Nature* **2005**, *438*, 201.
- [6] A. A. Balandin, S. Ghosh, W. Z. Bao, I. Calizo, D. Teweldebrhan, F. Miao, C. N. Lau, *Nano Lett.* **2008**, *8*, 902.
- [7] C. Lee, X. D. Wei, J. W. Kysar, J. Hone, *Science* **2008**, *321*, 385.
- [8] C. Gomez-Navarro, M. Burghard, K. Kern, *Nano Lett.* **2008**, *8*, 2045.
- [9] D. Li, R. B. Kaner, *Science* **2008**, *320*, 1170.
- [10] M. C. Lemme, T. J. Echtermeyer, M. Baus, H. A. Kurz, *IEEE Electron Device Lett.* **2007**, *28*, 282.
- [11] S. Gilje, S. Han, M. Wang, K. L. Wang, R. B. Kaner, *Nano Lett.* **2007**, *7*, 3394.
- [12] H. A. Becerril, J. Mao, Z. Liu, R. M. Stoltenberg, Z. Bao, Y. Chen, *ACS Nano* **2008**, *2*, 463.
- [13] G. Eda, G. Fanchini, M. Chhowalla, *Nat. Nanotechnol.* **2008**, *3*, 270.
- [14] J. S. Bunch, A. M. van der Zande, S. S. Verbridge, I. W. Frank, D. M. Tanenbaum, J. M. Parpia, H. G. Craighead, P. L. McEuen, *Science* **2007**, *315*, 490.
- [15] Z. Liu, J. T. Robinson, X. M. Sun, H. J. Dai, *J. Am. Chem. Soc.* **2008**, *130*, 10876.
- [16] J. C. Charlier, X. Gonze, J. P. Michenaud, *Phys. Rev. B* **1991**, *43*, 4579.

- [17] Z. F. Liu, Q. Liu, X. Y. Zhang, Y. Huang, Y. F. Ma, S. G. Yin, Y. S. Chen, *Adv. Mater.* **2008**, *20*, 3924.
- [18] Y. F. Xu, Z. B. Liu, X. L. Zhang, Y. Wang, J. G. Tian, Y. Huang, Y. F. Ma, X. Y. Zhang, Y. S. Chen, *Adv. Mater.* in press.
- [19] F. T. Vasko, V. Ryzhii, *Phys. Rev. B* **2008**, *77*, 195433.
- [20] K. F. Mak, M. Y. Sfeir, Y. Wu, C. H. Lui, J. A. Misewich, T. F. Heinz, *Phys. Rev. Lett.* **2008**, *101*, 196405.
- [21] S. X. Lu, B. Panchapakesan, *Nanotechnology* **2006**, *17*, 1843.
- [22] I. A. Levitsky, W. B. Euler, *Appl. Phys. Lett.* **2003**, *83*, 1857.
- [23] A. Fujiwara, Y. Matsuoka, H. Suematsu, N. Ogawa, K. Miyano, H. Kataura, Y. Maniwa, S. Suzuki, Y. Achiba, *Jpn. J. Appl. Phys.* **2001**, *40*, L1229.
- [24] P. C. Collins, M. S. Arnold, P. Avouris, *Science* **2001**, *292*, 706.
- [25] W. S. Hummers, R. E. Offeman, *J. Am. Chem. Soc.* **1958**, *80*, 1339.
- [26] S. Stankovich, D. A. Dikin, G. H. B. Dommett, K. M. Kohlhaas, E. J. Zimney, E. A. Stach, R. D. Piner, S. T. Nguyen, R. S. Ruoff, *Nature* **2006**, *442*, 282.
- [27] X. Wang, L. J. Zhi, K. Mullen, *Nano Lett.* **2008**, *8*, 323.
- [28] F. Tuinstra, J. L. Koenig, *J. Chem. Phys.* **1970**, *53*, 1126.
- [29] S. Stankovich, D. A. Dikin, R. D. Piner, K. A. Kohlhaas, A. Kleinhammes, Y. Jia, Y. Wu, S. T. Nguyen, R. S. Ruoff, *Carbon* **2007**, *45*, 1558.
- [30] J. S. Wu, W. Pisula, K. Mullen, *Chem. Rev.* **2007**, *107*, 718.
- [31] L. Onsager, *Phys. Rev.* **1938**, *54*, 554.
- [32] C. L. Braun, *J. Chem. Phys.* **1984**, *80*, 4157.
- [33] Y. Wang, *Nature* **1992**, *356*, 585.
- [34] M. Freitag, Y. Martin, A. J. Misewich, R. Martel, P. Avouris, *Nano Lett.* **2003**, *3*, 1067.
- [35] N. S. Sariciftci, L. Smilowitz, A. J. Heeger, F. Wudl, *Science* **1992**, *258*, 1474.
- [36] G. Dicker, T. J. Savenije, B. H. Huisman, D. M. de Leeuw, M. P. de Haas, J. M. Warman, *Synth. Met.* **2003**, *137*, 863.
- [37] H. Noriaki, S. Shin-ichi, O. Atsushi, *Phys. Rev. Lett.* **1992**, *68*, 1579.
- [38] M. Hirata, T. Gotou, M. Ohba, *Carbon* **2005**, *43*, 503.
- [39] X. Lv, F. Du, Y. F. Ma, Q. Wu, Y. S. Chen, *Carbon* **2005**, *43*, 2020.

Received: January 8, 2009  
Revised: February 23, 2009  
Published online: